Journal of the Textile Institute

Development of mathematical model to predict vertical wicking behaviour. Part I: flow through yarn

Brojeswari Das [a] , Apurba Das [a] , Vijay K. Kothari [a] & Raul Fangueiro [b]

[a] Department of Textile Technology, Indian Institute of Technology, Delhi, India

[b] Department of Textile Engineering, University of Minho, Guimarães, Portugal

PLEASE SCROLL DOWN FOR ARTICLE

Taylor & Francis
Taylor & Francis Group

Development of mathematical model to predict vertical wicking behaviour. Part I: flow through yarn

Brojeswari Das[a], Apurba Das[a]*, Vijay K. Kothari[a] and Raul Fangueiro[b]

[a]Department of Textile Technology, Indian Institute of Technology, Delhi, India; [b]Department of Textile Engineering, University of Minho, Guimarães, Portugal

Theoretical models have been proposed in this article (Parts I and II) to predict the vertical wicking behaviour of yarns and fabrics based on different fibre, yarn and fabric parameters. The first part of this article deals with the modelling of flow through yarn during vertical wicking, whereas the second part deals with the modelling of vertical wicking through the fabric. The yarn model has been developed based on the Laplace equation and the Hagen–Poiseuille's equation on fluid flow; pore geometry has been determined as per the yarn structure. Factors such as fibre contact angle, number of filaments in a yarn, fibre denier, fibre cross-sectional shape, yarn denier and twist level in the yarn have been taken into account for development of the model. Lambertw, a mathematical function, has been incorporated, which helps to predict vertical wicking height at any given time, considering the gravitational effects. Experimental verification of the model has been carried out using polyester yarns. The model was found to predict the wicking height with time through the yarns with reasonable accuracy. Based on the proposed yarn model, a mathematical model has been developed to predict the vertical wicking through plain woven fabric in the second part of this article.

Keywords: vertical wicking; capillary action; Laplace equation; Hagen–Poiseuille's equation; Lambertw function

Nomenclature

N	Total number of fibres in yarn
P	Total number of pores in yarn
i	Number of fibre layers in yarn
R_f	Fibre radius (cm)
μ	Yarn packing co-efficient
x	Distance between two fibres (cm)
a	Distance between nearest fibres' axis (cm)
P_{sp}	Perimeter of single capillary (cm)
A_{sp}	Area of single capillary (cm^2)
P_p	Total perimeter of capillary (cm)
A_p	Total area of capillary (cm^2)
γ_{SV}	Surface tension between solid and vapour interface (dyne/cm)
γ_{SL}	Surface tension between solid and liquid interface (dyne/cm)
γ_{LV}	Surface tension between liquid and vapour interface (dyne/cm)
θ	Contact angle (radian)
A	Adhesive force between solid and liquid molecule (dyne)
τ	Tension acting on the liquid surface (dyne/cm)
P_c	Capillary pressure (dyne/cm^2)
r	Radius of the capillary (cm)
R	Curvature of the capillary meniscus (cm^{-1})
R_y	Yarn radius (cm)
n	Number of fibres in the outer layer of yarn
T	Twist per unit length in the yarn (turns/cm)
H	Pitch length (cm)
r_y	Radius of fibre helical path (cm)
dr_y	Elemental yarn radius (cm)
dn	Number of fibres in the elemental sectional of the yarn
α	Helix angle of fibre in the yarn (radian)
ΔP	Pressure difference
η	Viscosity of the liquid (centipoise)
Q	Flow rate (wicking height/time)
D_H	Hydraulic diameter of capillary (cm)
ϕ	Angle of occurrence of liquid meniscus with the outer layer fibre wall (radian)
L_f	Fibre length (cm)
A_f	Fibre area (cm^2)
P_f	Fibre perimeter (cm)
P_{cir}	Perimeter of circle having same area of the fibre cross-section (cm)
ρ_f	Fibre density (g/c.c.)
d	Fibre denier
χ	Fibre shape factor
t	Time of wicking (s)
ρ	Density of liquid (g/c.c.)
g	Gravitational acceleration (dynes/cm^2)
m	Mass of the liquid column (g)
h_{max}	Equilibrium capillary height (cm)
h	Yarn wicking height (cm)

*Corresponding author. Email: apurba@textile.iitd.ernet.in

Ap_{warp}	Cross-sectional area of pore in warp way (cm^2)
Ap_{weft}	Cross-sectional area of pore in weft way (cm^2)
h_{fab}	Fabric wicking height (cm)
l	Total wicking length along the fabric (cm)
p_1, p_2	Warp and weft spacing (cm)
n_2	Number of weft threads at h_{fab} distance (cm)
c_1, c_2	Warp and weft crimp
α_1, α_2	Warp and weft crimp angle (radian)
l_1, l_2	Lengths of the thread axis between planes containing the axes of consecutive cross-threads (cm)

Introduction

Influence of various factors and prediction of moisture transmission behaviour of the clothing has been recognised as a favourite research arena among the research fraternity in recent years. Theoretical prediction of moisture transmission properties of textile materials is useful to characterise the clothing comfort, and also it helps to design the fabric as per specifications. Liquid moisture wicking behaviour of fabric plays an important role in maintaining thermophysiological clothing comfort, especially in sweating conditions. The procedures adopted to characterise the liquid moisture transmission behaviour of fabrics are transverse wicking, in-plane wicking and vertical wicking methods. The reported theoretical works on liquid moisture transfer through fabrics are found to be concentrated on in-plane wicking and transverse wicking studies. No theoretical work has been reported to predict the vertical wicking through fabric, though it is a most commonly used method to determine the wickability. Yarn is the key factor in determining wicking behaviour of fabric. Hence, the necessity of a theoretical model to predict the vertical wicking behaviour of yarn and fabric with known material parameters has been recognised and attempted in this study. The theoretical background of the capillary action through textile structure has been given below.

Capillarity and textile structure

Capillary action, or capillarity, can be defined as the macroscopic motion or flow of a liquid under the influence of its own surface and interfacial forces. It is based on the intermolecular forces of cohesion and adhesion. During wetting, the forces at equilibrium between solid–liquid boundaries are commonly described by the Young–Dupre equation (1), as given below (Kissa, 1996):

$$\gamma_{SV} - \gamma_{SL} = \gamma_{LV} \cos \theta \cdot \qquad (1)$$

When liquid wets the fibres, it reaches the spaces between the fibres, and capillary pressure develops. The

liquid is forced by this pressure and dragged along the capillary due to the curvature of meniscus in the narrow confines of the pores. The spontaneous flow of liquid or wicking occurs due to a pressure differential or capillary action. The magnitude of the capillary pressure is given by Laplace equation (2) (Chatterjee, 1985):

$$P_c = \frac{2\gamma_{LV} \cos \theta}{r} \cdot \qquad (2)$$

With an idealised tube structure, the Hagen–Poiseuille law (Hagen, 1839) for laminar flow through a circular tube is employed, as per the following equation:

$$Q = \frac{dh}{dt} = \frac{r^2}{8\eta} \times \frac{\Delta P}{h} \cdot \qquad (3)$$

This equation is also used for the steady state flow through a porous media. In such cases, to define the pore diameter, hydraulic diameter of pore is considered and calculated on account of non-circularity and irregularity in the pore structure and spacing (Lekner, 2007; Millionshchikov, 1970). The capillary rise between the time of initial contact and the final equilibrium was obtained by integrating Equation (3) as derived by Lukas–Washburn (Lukas, 1918; Washburn, 1921).

$$\ln\left(1 - \frac{h}{h_{max}}\right)^{-1} - \frac{h}{h_{max}} = Ct \qquad (4)$$

C is constant. At low values of t, where h is very small comparative to the h_{max}, the above equation has been approximated as follows to establish the direct relation between wicking height (h) and the wicking time (t), commonly known as Washburn equation (Washburn, 1921).

$$h = \sqrt{\frac{r\gamma \cos \theta}{2\eta} \times t} \qquad (5)$$

Washburn equation is the only available equation till the date which directly provides the wicking height through a capillary channel for specified time t. The main limitation in case of vertical wicking of this equation is that it is only valid for very low values of t and not for the complete wicking profile.

In case of textile yarns, the pores are open channel capillaries formed by the fibre walls unlike the regular capillary channel (Mao & Russell, 2000; Minor & Schwartz, 1960). The capillaries are neither cylindrical nor all of them are arranged in parallel. The size and the

shape of the capillaries are dependent on the size and the shape of the fibres as well their packing in yarn. So the different fibre and yarn parameters which affect the shape, size and distribution of the capillaries are likely to affect the capillary drag through the yarn structure. Involvement of so many variables and the irregular capillary structure complicates the model of flow through the textile structure. The theoretical studies, conducted by different researchers to study the wicking behaviour through textile yarns, either treat the yarn as porous media, where the liquid transport process can be described by Darcy's law (Chatterjee, 1985), or as capillary tubes (Kamath, Hornby, Weigman, & Wilde, 1994; Liu, Choi, & Li, 2008; Nyoni & Brook, 2006; Palmer, 1953; Perwuelz, Casetta, Caze, 2000; Perwuelz, Mondon, & Caze, 2001; Wiener & Dejlová, 2003), where the liquid flow through can be modelled by Lucas–Washburn kinetics. But as discussed by Wiener and Dejlová (2003) in most of the theoretical works, to simplify the case many important parameters and phenomenon have been overlooked, which leads to output with higher error percentage. Wiener and Dejlová (2003) have developed a model which can predict the equilibrium wicking height considering the following textile parameters: fineness of fibres and number of fibres at the cross-section in the bundle and the filling. Liu et al. (2008) proposed a mathematical model on wicking through twisted yarn based on idealised yarn structure model (Hearle, Grosberg, & Baker, 1969). The equilibrium height of wicking as proposed by the model was observed to diverge with the experimental results of the article. In most of the works only the equilibrium wicking height through the yarn has been calculated rather than the complete wicking profile, where the gravitation force has to be taken into account at every point. Neither correlation with yarn and fabric wicking has been quantifiable in the substantial published research works.

In the present part of this article, a mathematical model has been developed to predict the complete profile of vertical wicking through yarn considering different influencing parameters, i.e. fibre contact angle, number of filaments in a yarn, fibre denier, fibre cross-sectional shape, yarn denier and twist level in the yarn.

Model development

The proposed model is based on Laplace and Hagen–Poiseuille equation. The salient features of this model are:

- Yarns are considered as porous materials comprising irregular cylindrical fibres and air;
- The capillaries in yarn are open channel capillaries, comprised of fibre wall;

- The available fibre wall to a capillary channel drags water along it, and the proportion of the wall to a capillary channel depends on yarn packing co-efficient; and
- The gravitational force acts downward to resist the flow through the channel.

Development of a mathematical model to predict the vertical wicking through yarn has been achieved in different stages. The first stage comprises of defining the pore geometry, the number of pores in the yarn and the number of fibres at the outer layer of yarn. The second stage deals with capillary flow calculation. In the third and the fourth stages, yarn twist parameter and fibre shape factors successively have been incorporated in the yarn model. The developed yarn model has been verified with the experimental results.

Stage 1: defining pore geometry

To define pore geometry, at the initial stage, the following assumptions have been considered:

- The fibres in the yarn are hexagonally packed;
- All fibres are of same dimension;
- All the fibres are equally spaced; and
- The cross-section of the fibres is circular.

Determination of the number of pores in the yarn structure

To determine the number of pores in the yarn structure, a hexagonal close packing has been assumed. With the change in packing, the co-efficient number of pores will not change, only the area and perimeter of the pores will change. In case of hexagonal close packing, the number of fibres in the core = 1. Here in the article, i is the number of fibre layers in the yarn. The number of fibres in different fibre layers in the yarn in case of hexagonal close packing according to Hearle et al. (1969) has been given in Table 1.

The total number of fibres in a yarn with i number of fibre layers is as follows:

$$N = 1 + 6 + 12 + 18 + 24 + 30 + \ldots + N_{i\text{th}}$$

$$N = 1 + 3i + 3i^2 \tag{6}$$

$$i = \frac{-3 + \sqrt{12N - 3}}{6} \tag{7}$$

where $N_{i\text{th}}$ is the number of fibres in the ith layer.

Table 1. Hexagonal close packing of fibres in yarn.

No. of layer (i)	No. of fibres in the layer (N_i)	Total number of fibres (N)
0	1	1
1	6	7
2	12	19
3	18	37
4	24	61
5	30	91

Table 2. Number of pores formed by different fibre layers.

No. of layer (i)	No. of pores for the layer	Total number of pores (P)
0	0	0
1	6	6
2	6 + 12 = 18	24
3	12 + 18 = 30	54
4	18 + 24 = 42	96
5	24 + 30 = 54	150
6	30 + 36 = 66	216

The number of pores form in the yarn structure due to different fibre layers has been given in Table 2.
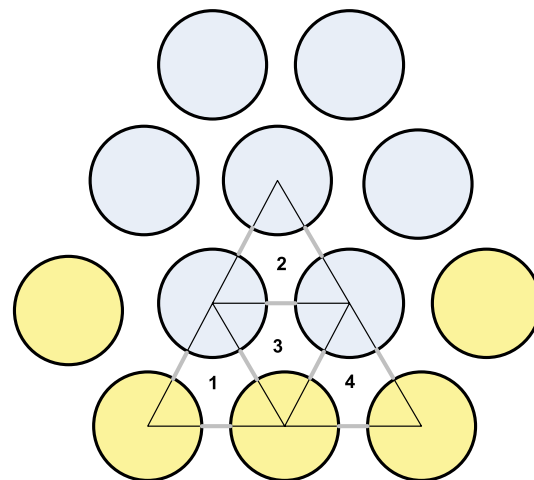
The total number of pores, P, in the yarn with i number of layers:

$$6 + 18 + 30 + 42 + 54 + 66 + \ldots + \text{number of pores}$$
$$\text{for } i\text{th layer } P = 6i^2$$
$$\Rightarrow P = \frac{\left(-3 + \sqrt{12N - 3}\right)^2}{6}. \qquad (8)$$

Determination of pore dimension

The geometrical dimension of pore has been defined in two different ways. In the first approach, an individual pore, as shown in Figure 1(a) and (b), has been considered. In second approach, the total number of pores has been considered as a unit porous system (Figure 3).

In case of textile material, the pores formed between fibres are open channel capillary, constructed by the fibre walls. In an open-packed yarn, the pores can be geometrically presented by the combination of real fibre border (line in black) and by the fictive border (line in grey) (Neckar & Ibrahim, 2003). In case of an open-packed yarn, the number of pores is going to be same as that in close packed. The perimeter offered by the solid surface to wetting is also going to be the same. Only the pore area and the perimeter (imaginary perimeter of a single pore) will be different. The geometrical pore dimensions have been marked in Figure 2.

$$\text{Packing co-efficient of yarn, } \mu = \frac{\text{Area accupied by fibre}}{\text{Yarn area}}$$

$$= \frac{\text{Fibre area}}{\text{Total area}}$$

Considering the portion of ΔABC in Figure 2:

$$\mu = \frac{\frac{3}{6} \times \pi R^2{}_f}{\frac{\sqrt{3}}{4} \times a^2}$$

(a) Close packing   (b) Open packing

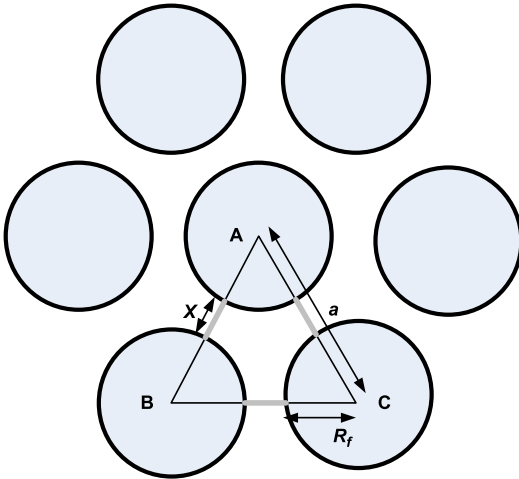Figure 1. Pore structure in hexagonally packed yarn.

Figure 2. Geometrical dimension of pore.

$$a = 1.075 \sqrt{\frac{\pi R_f^2}{\mu}}$$

$$x = a - 2 \times R_f = \frac{1.903}{\sqrt{\mu}} R_f - 2R_f = \left(\frac{1.903}{\sqrt{\mu}} - 2\right) R_f$$

So, the area of the single capillary $(A_{sp}) = \frac{\pi R_f^2}{2} \times \frac{1-\mu}{\mu}$.

The solid fibre surface available to the capillary to raise the liquid, the wetted perimeter of the channel is as follows:

$$P_{sp} = \pi R_f \qquad (9)$$

$$D_H = \frac{4 A_{sp}}{P_{sp}} \qquad (10)$$

where A_{sp}, P_{sp} and D_H are the area, the wetted perimeter and the hydraulic diameter of the pore.

Determination of the number of fibres in outer layer of yarn

From Equation (7), when i comes as a whole number, then the yarn has i number of complete fibre layers. If i comes with a fraction, then total number of complete fibre layer will be the nearest lower whole number (suppose K) and the next fibre layer will be incomplete.

In that case K is the number of complete layer and $(K + 1)$th is the last and incomplete fibre layer.

In this packing system, the number of fibres in Kth layer is $6K$.

The number of fibres in the last layer $(K + 1)$:

$$J = N - (1 + 3K + 3K^2) \cdot$$

The number of fibres in $(K + 1)$ layer will cover $J \times \dfrac{K}{K+1}$ number of fibres of Kth layer.

Therefore, the total number of fibres in the outside surface of the yarn (n) will be:

$$n = 6K + \frac{J}{K+1}. \qquad (11)$$

Stage 2: capillary flow calculation

Capillary pressure can be determined by two ways. Approach 1: in this approach single pore (dimensionally) has been used. In this approach the fictive borders between the pores has been considered to separate one pore from the adjacent, and the number of pores and pore dimension have been determined from the previous calculations. Approach 2: in this approach the total number of pores has been considered as a unit porous system. The imaginary borders between the pores have not been considered, and the capillary pressure can be calculated using total capillary force and total capillary area present in the yarn, rather than considering the individual capillaries.

Calculation considering individual pore

Forces acting during the vertical capillary flow through a capillary channel are the upward acting capillary force and the downward acting gravimetric force.

So the pressure difference is:

$$\Delta P = \frac{2\pi r \gamma_{LV} \cos\theta - mg}{\pi r^2}$$
$$= (P_c - h\rho g) \qquad (12)$$

where ΔP is the pressure difference, ρ is the density of the liquid, m is the mass of the liquid, wicked along the channel and g is the gravitational acceleration.

At the equilibrium height (h_{max}), ΔP will be zero in the condition:

$$h_{max} = \frac{P_c}{\rho g}. \qquad (13)$$

In case of non-circular capillary, r is replaced by $D_H/2$ (Lekner, 2007; Millionshchikov, 1970). Now placing the value of ΔP (Equation (12)) in Hagen–Poiseuille equation (Equation (3))

$$\frac{dh}{dt} = \frac{\left(\frac{D_H}{2}\right)^2}{8\eta} \times \frac{\Delta P}{h} = \frac{\left(\frac{D_H}{2}\right)^2}{8\eta h}$$

$$\times \frac{(\text{Capillary force} - \text{Gravitational force})}{A_{sp}}$$

$$\frac{dh}{dt} = B\left(\frac{k}{h} - 1\right) \qquad (14)$$

where $B = \dfrac{\left(\dfrac{D_H}{2}\right)^2}{8\eta}\rho g, k = \dfrac{\text{Capillary pressure}}{\rho g} = h_{max}$

$$\text{Capillary pressure}: P_c = \frac{2\gamma_{LV}\cos\theta \times \mu}{(1-\mu)R_f}$$

$$\text{Hydraulic diameter}: D_H = \frac{2 \times R_f \times (1-\mu)}{\mu}$$

(using the values of A_{sp} and P_{sp} from the previous calculations).

Equation (14) has been integrated for time t as follows:

$$\int_0^h \frac{dh}{\left(\frac{k}{h} - 1\right)} = \int_0^t B\,dt \qquad (15)$$

The integration gives a non-linear equation relating wicking height h and time t as follows:

$$Bt + k\log\left(1 - \frac{h}{k}\right) + h = 0 \cdot \qquad (16)$$

The non-linear equation has been solved using MATLAB, which has given following solution. From this equation, the value of the wicking height h can be determined for any time t:

$$h = k\{\text{Lambertw}(-e^{-(k+Bt)/k}) + 1\} \qquad (17)$$

Lambertw is a mathematical function defined as follows:

$w = \text{Lambertw}(x)$ is the solution to $w \times \exp(w) = x$.

The limitations in determining the capillary force by Approach 1

- This approach cannot take care of irregular spacing between the fibres, as well as the way in which the pore's dimension has been measured, is only valid for regular shaped fibre – such as circular, square-shaped, rectangular, triangular, etc.
- This approach cannot take care of the cohesive force, acting downward, due to the concave liquid–gas interface which leads to higher error percentage.

So the second approach has been used for the final model.

Calculation considering total number of pores as unit porous system

In this approach the imaginary borders between the capillaries have not been considered (Figure 3), and the capillary pressure has been calculated using total capillary force and total capillary area present in the yarn, rather than considering the individual capillaries.

In this case the total area of capillary is:

$$A_P = \pi R_y^2 \times (1-\mu) \qquad (18)$$

where R_y is the yarn radius.
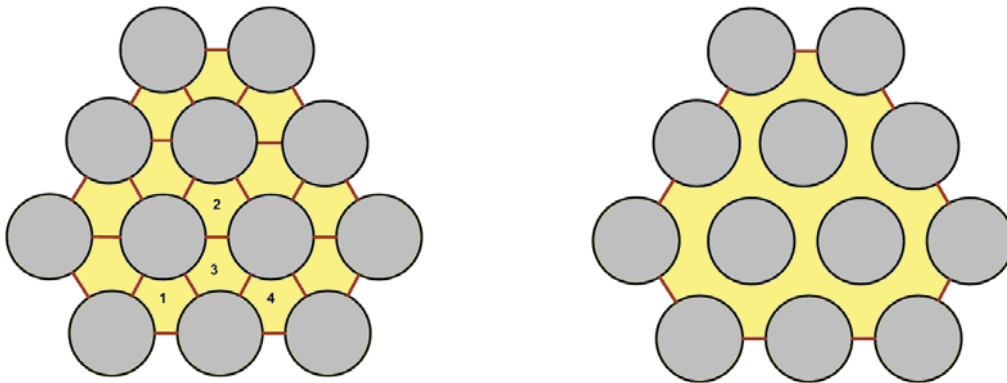

Figure 3.   Removal of fictive borders.

Wetted perimeter of the capillary = total number of fibres × perimeter of a fibre – number of fibres at the outer layer of yarn × perimeter of non – wetted fibre portion (19)

Effective capillary force acting upward =

$\gamma_{LV} \cos\theta \times$ (perimeter of total number of fibres in the yarn – fibre perimter not in contact of water) $-\gamma_{LV} \times$ non – wetting liquid perimeter (20)

Clark and Millar (1978) have worked to determine the liquid meniscus in a cross-sectional plane. They have calculated the point of occurrence of the liquid curvature and its shape between two fibres which are at the outer plane of the yarn.

The radius of curvature of the liquid meniscus (R) (Figure 4):

$$R_f \left[\frac{(F+1) - \sin\phi}{\sin(\phi + \theta)} \right] \qquad (21)$$

where $F = \dfrac{x}{2R_f}$ and

$$\phi = \cos^{-1} \left[\frac{-\sin\theta\cos\theta \pm \sin\theta \sqrt{(F+1)^2 - \sin^2\theta}}{(F+1)} \right]$$

(The details of calculation have been given by Clark and Miller, 1978.)

The length of the arc (S)

$$= R \times 2(\pi - \theta - \phi)$$
$$= 2R_f \left[\frac{(F+1) - \sin\phi}{\sin(\phi + \theta)} \right] \times (\pi - \theta - \phi). \qquad (22)$$

The perimeter of the non-wetted fibre portion is:

$$2(\pi - \phi) \times R_f. \qquad (23)$$

Hence, the deduction of capillary force due the non-wetted fibre portion (F_{du1}) is:

$$2(\pi - \phi) \times R_f \times n \times \gamma_{LV} \times \cos\theta \qquad (24)$$

and the downward force by non-wetting water perimeter (F_{du2}) is:

$$2R_f \left[\frac{(F+1) - \sin\phi}{\sin(\phi + \theta)} \right] \times (\pi - \theta - \phi) \times n \times \gamma_{LV}. \qquad (25)$$

Therefore, the total capillary force (F_c) obtained is as follows:

$$F_c = (N \times 2\pi R_f - 2(\pi - \phi) \times R_f \times n)\gamma_{LV} \cos\theta - 2R_f$$
$$\left[\frac{(F+1) - \sin\phi}{\sin(\phi + \theta)} \right] \times (\pi - \theta - \phi) \times n \times \gamma_{LV}. \qquad (26)$$

Stage 3: incorporation of twist parameter in yarn modelling

Liu et al. (2008) have used the idealised yarn structure model developed by Hearle et al. (1969) to determine
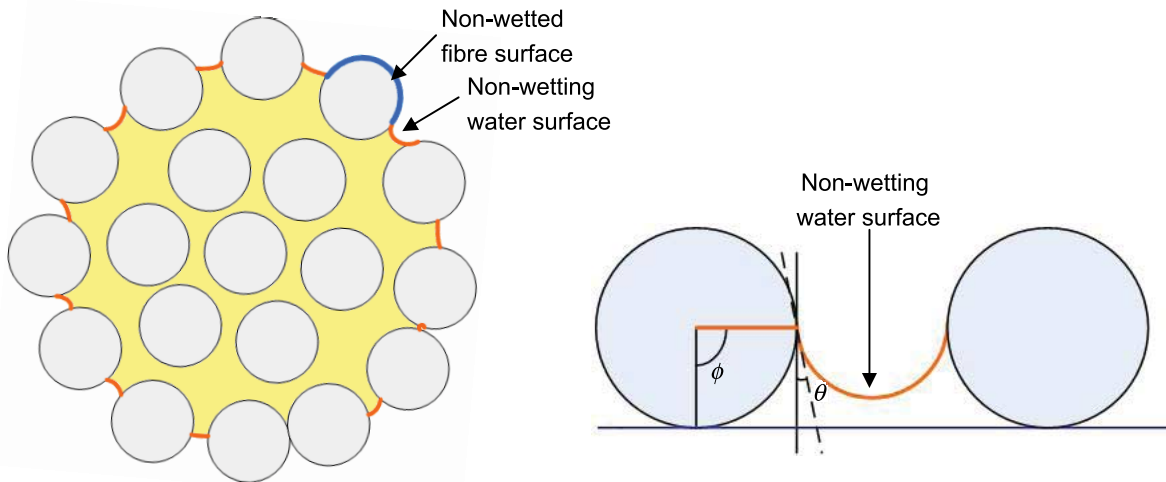

Figure 4.   Formation of non-wetting water surface at the outer layer of yarn.

the fibre inclination in the elemental area and their contribution to the capillary dragging in case of twisted. The same concept has been used in our model as well.

The yarn is assumed to be circular in cross-section, and composed of a series of concentric cylinders of differing radius. Each fibre follows a uniform helical path around one of the concentric cylinders, so that its distance from the yarn axis remains constant. All such helices have the same pitch. A typical constitute fibre is shown in Figure 5. Since fibres within the yarn are not parallel to each other any more, inclinations of fibres to the vertical line (α) should be taken into account. Without losing generality, only one pitch of the yarn is considered in the analysis. Considering an element of area of cross-section of the yarn between radii r_y and r_y + dr_y and supposing packing of fibres in the yarn is uniform, the number of composed fibres inside this area can dn be obtained by:

$$dn = \frac{\mu \cdot 2\pi r_y dr_y \cdot H}{\pi R_f^2 \cdot L_f} = \frac{2\mu r_y dr}{R_f^2 \sqrt{1 + 4\pi^2 r_y^2 T^2}} \qquad (27)$$

(The calculation which has been given by Liu et al. (2008) has been corrected here.)

where μ is the packing fraction of fibres in the yarn, r_y is the radius of the fibre helical path, H is the pitch length of the helix of the fibre path, T is the twist in the yarn per unit length, R_f is the average radius of fibre and L_f is the fibre length.

$$H = \frac{1}{T}.$$

The upward capillary force contributed by this element area is therefore given by:
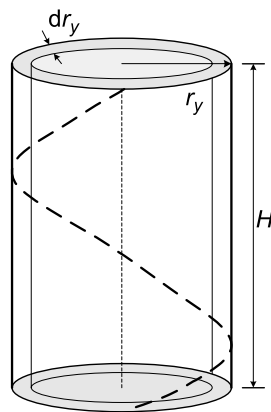
$$dF_{cu} = 2\pi R_f \cdot dn \cdot \gamma_{LV} \cos(\theta + \alpha)$$
$$= \frac{4\pi\mu\gamma_{LV} r_y dr_y \cos(\theta + \alpha)}{R_f \sqrt{1 + 4\pi^2 r_y^2 T^2}} \qquad (28)$$

where α is the twist angle.

$$\alpha = \cos^{-1}\left(\frac{1}{\sqrt{1 + 4\pi^2 r_y^2 T^2}}\right).$$

By integrating the Equation (28) over the yarn radius, we will get the total upward force in the yarn wicking as such:

$$F_{cu} = \frac{4\pi\mu\gamma_{LV}}{R_f} \int_0^{R_y} \frac{r_y \cos(\theta + \alpha)}{\sqrt{1 + 4\pi^2 r_y^2 T^2}} \, dr_y$$
$$= \cos^{-1}\left(\frac{1}{\sqrt{1 + 4\pi^2 r_y^2 T^2}}\right). \qquad (29)$$

In the twisted condition, the deduction of capillary force due to the non-wetted fibre portion is:

$$(F_{du1}) = 2(\pi - \phi) \times R_f \times n \times \gamma_{LV}$$
$$\times \cos\left[\theta + \cos^{-1}\left(\frac{1}{\sqrt{1 + 4\pi^2 r_y^2 T^2}}\right)\right]. \qquad (30)$$

Downward force by non-wetting water perimeter (F_{du2}) is:

$$2R_f \left[\frac{(F+1) - \sin\phi}{\sin(\phi + \theta)}\right] \times (\pi - \theta - \phi) \times n \times \gamma_{LV}. \qquad (31)$$
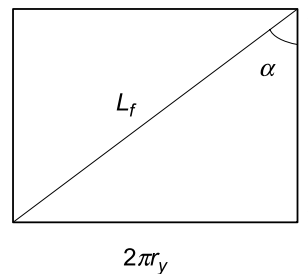

Figure 5.   Idealised structure of twisted yarn.

Therefore, the equivalent upward force for the wicking action is:

$$F_c = F_{cu} - (F_{du1} + F_{du2}). \qquad (32)$$

Also, to calculate the hydraulic diameter (D_H) of the pore, the overall pore area and wetted perimeter has been considered.

Stage 4: incorporation of fibre shape factor in yarn modelling

Normally, the difference in the cross-sectional shape of the fibres is quantified by the factor known as a shape factor. Shape factor of any cross-sectional shape is determined as follows:

$$\text{Shape factor } (\chi) = \frac{P_f}{P_{cir}} \qquad (33)$$

where P_f is the perimeter of that particular cross-sectional shape and P_{cir} is the perimeter of the circle having the same cross-sectional area of that particular shape.

With the same denier of the fibres having different cross-sectional shape, we will have same cross-sectional areas but different perimeters.

Therefore, if the denier of a fibre is d, the cross-sectional area of the fibre will be:

$$A_f = \frac{d}{\rho_f \times 9 \times 10^5}$$

$$P_{cir} = \sqrt{4\pi A_f}$$

$$P_f = \chi \sqrt{4\pi A_f}$$

In case of circular cross-sectional fibre, it will be:

$$R_f = \frac{2A_f}{P_f}. \qquad (34)$$

Therefore, in case of fibre with non-circular cross-section in all the above equations of previous part, R_f will be replaced by A_f and P_f (Equation (34)) of that particular cross-sectional fibre.

Experimental validation

Materials

In order to experimentally verify the yarn wicking model, polyester and polypropylene multifilament yarns have been used. Polyester filaments with three different cross-sectional shapes, i.e. circular, triangular and trilobal have been used to see the effect of shape factor on yarn wicking. Contact angle of the filament yarns has been measured using tensiometry method. Polyester multifilament yarns having similar denier but made of different denier per filaments have been used to study the effect of fibre diameter on yarn wicking. Different twist level has been incorporated on the multifilament polyester yarns to observe the effect of twist on yarn wicking. The diameter of the filament yarns and zero twist and twisted condition have been measured using Leica microscope. The details of yarn parameters have been given in Table 3.

Method

Measurement of vertical wicking vs. time

Vertical wicking height has been measured with respect to time using vertical wicking tester. The measurement has been done using video-metric method. The experimental set up has been given in Figure 6. The whole process from the starting of the wicking process till water reaches to the equilibrium in the yarn has been captured in video camera. 3 g/l Procion red reactive dye has been

Table 3.   Parameters of polyester yarns with microdenier filaments and different cross-sectional filaments.

Sample code	Fibre type	Cross-sectional shape	Fibre shape factor	Contact angle	Fibre denier	No. of filaments/yarn	Yarn denier	Yarn radius (cm)
Trilobal	Polyester	Trilobal	1.27	75.75	4.72	32	151	0.0073
Triangular	Polyester	Triangular	1.16	75.75	4.72	32	151	0.0073
Circular-normal denier	Polyester	Circular	1	75.75	4.72	32	151	0.0072
Microdenier	Polyester	Circular	1	70	0.84	200	167	0.0085
PET1	Polyester	Circular	1	70.96	5.26	220	1158	0.019
PET2	Polyester	Circular	1	63.28	5.26	190	1000	0.018
PP1	Polypropelene	Circular	1	60.45	9.5	115	1100	0.022
PP2	Polypropelene	Circular	1	45.20	10	86	862	0.020
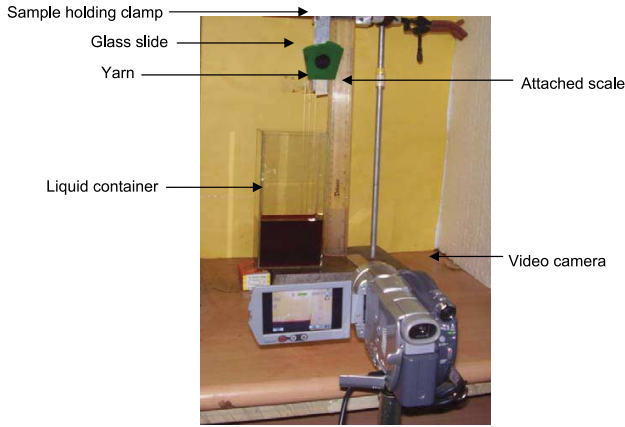
Figure 6. Experimental set-up for measuring vertical wicking of yarn and fabric.

Figure 8. Comparison of wicking height obtained from the vertical wicking test and the theoretical model.

added in water, which has been used for the experiment, to improve the visual clarity of the flow. In order to verify the twist effect on yarn wicking, different ranges of twist were imparted on the multifilament yarns.

Comparison of theoretical and experimental values

Based on the mathematical model, a programme has been made using MATLAB software to obtain the complete vertical wicking profile (height from the initial to wicking equilibrium) of yarn just by entering the fibre and yarn parameters as input variables. The values obtained from the yarn model have been compared with the wicking height values obtained from vertical wicking test. It can be observed from Figure 7 that the R^2 value between the experimental and theoretical wicking height is high, which indicates that both the theoretical and the experimental results follow the same trend. Table 4 gives a comparison of the values of maximum wicking height values of the different yarns obtained from the experiment and the model. The error percentage between the theoretical
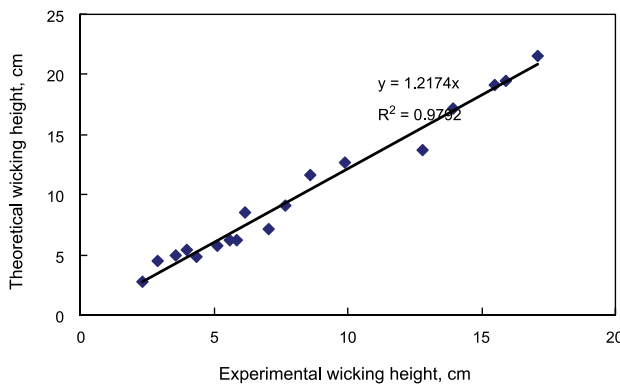

Figure 9. Comparison of theoretical and experimental wicking height through circular microdenier multifilament polyester yarn. e, experimental; t, theoretical.

Figure 7. Correlation between the values obtained from vertical wicking test and the theoretical model.

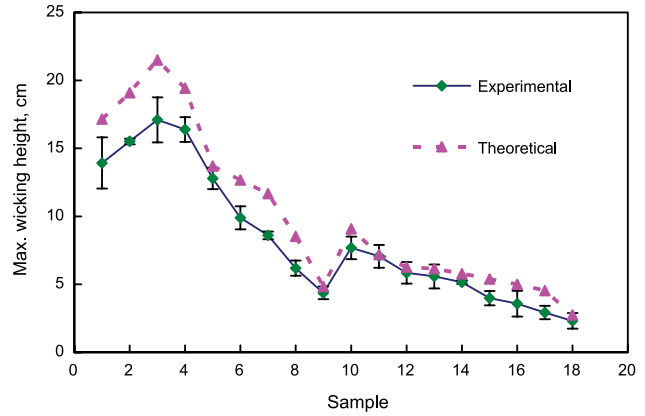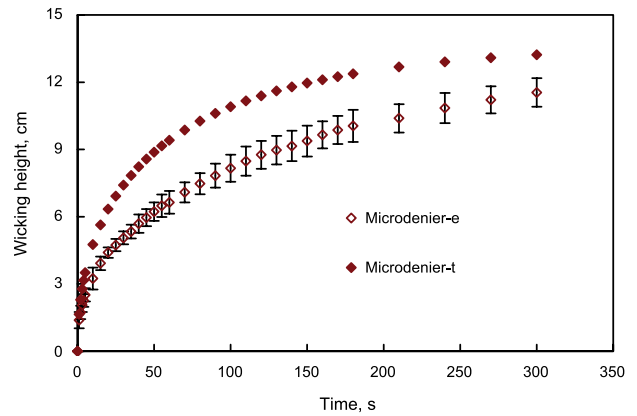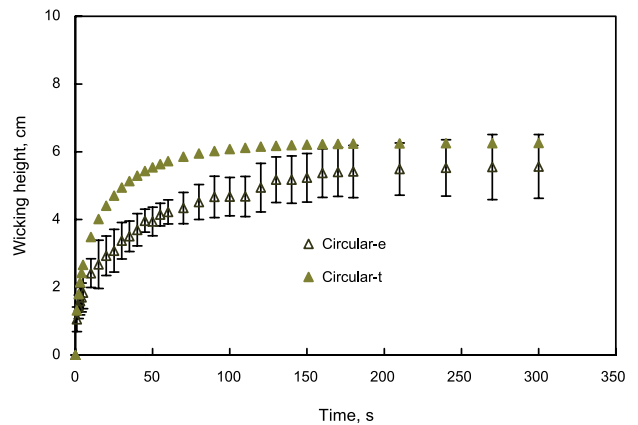Figure 10. Comparison of theoretical and experimental wicking height through circular normal denier multifilament polyester yarn. e, experimental; t, theoretical.
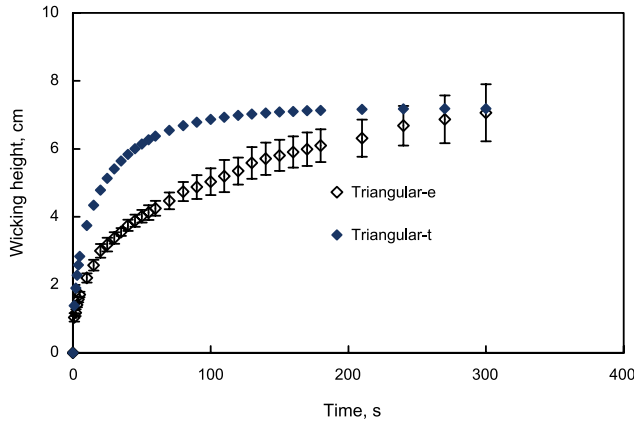
Figure 11. Comparison of theoretical and experimental wicking height through triangular multifilament polyester yarn. e, experimental; t, theoretical.

Figure 12. Comparison of theoretical and experimental wicking height through trilobal multifilament polyester yarn. e, experimental; t, theoretical.

and the experimental values has been calculated. From the results it has been seen that the model can predict the wicking values with reasonable accuracy. Figure 8 gives a comparative display of the values obtained from the experiment and the proposed model. The theoretical and the experimental wicking height through different denier and different cross-sectional multifilament polyester yarns have been 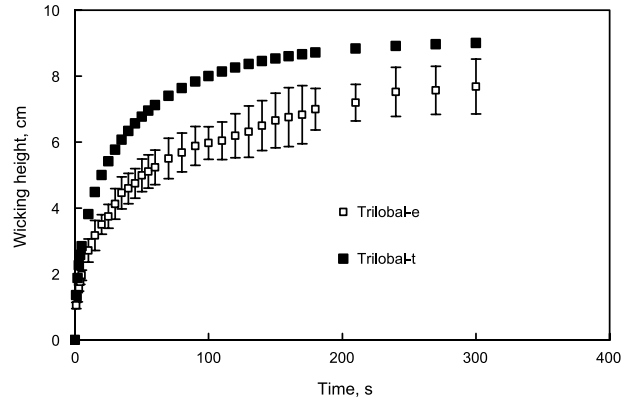compared in Figures 9–12. The error bars given in the graphs represent the standard deviation between the measured values of a sample.

Effect of fibre diameter

The effect of fibre diameter on vertical wicking behaviour of yarn has been plotted in Figure 13(a) and (b). From the plots it is observed that the result obtained from the model as well as the experiment follow the same trend; in case of microdenier filament yarn, the

Table 4. Comparison of theoretical and experimental values.

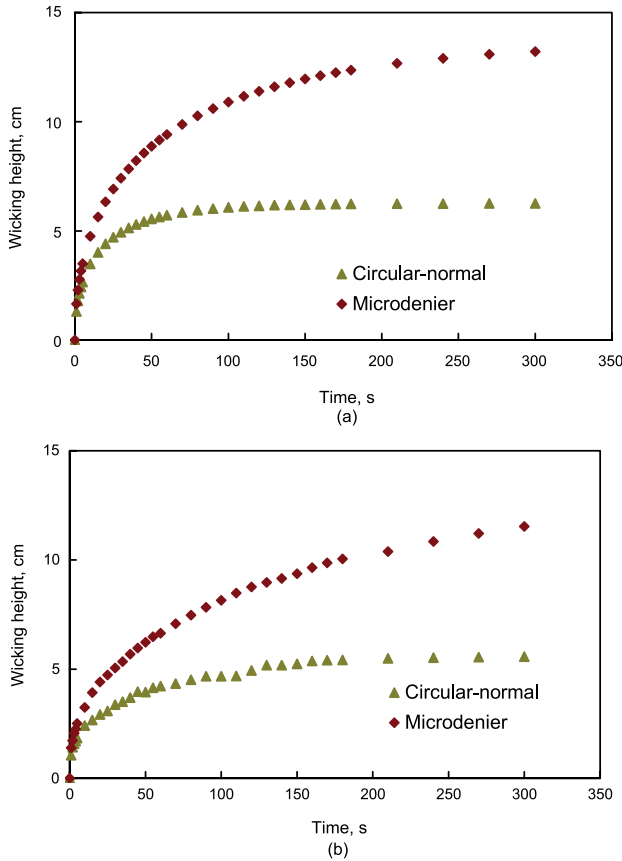| Sr. No.	Yarn type	Experimental max. wicking height, cm (h_E)	Predicted max. wicking height, cm (h_T)	Error $\dfrac{\lvert h_E - h_T \rvert}{h_E}$
1	PET1	13.93	17.17	0.23
2	PET2	15.52	19.10	0.23
3	PP1	17.10	21.50	0.26
4	PP2	15.90	19.43	0.22
5	Microdenier-twist-0	12.80	13.71	0.07
6	Microdenier-1 TPCM	9.90	12.68	0.28
7	Microdenier-2 TPCM	8.60	11.68	0.36
8	Microdenier-5 TPCM	6.19	8.54	0.38
9	Microdenier-10 TPCM	4.37	4.84	0.11
10	Trilobal	7.68	9.09	0.18
11	Triangular	7.06	7.19	0.02
12	Circular-normal denier-0 TPCM	5.85	6.26	0.07
13	Circular-normal denier-1 TPCM	5.58	6.17	0.11
14	Circular-normal denier-2 TPCM	5.15	5.78	0.12
15	Circular-normal denier-3 TPCM	3.98	5.40	0.36
16	Circular-normal denier-4 TPCM	3.57	4.99	0.40
17	Circular-normal denier-5 TPCM	2.92	4.54	0.56
18	Circular-normal denier-10 TPCM	2.31	2.74	0.19
			Average	0.23
			Max	0.56
			Min	0.02

Note: TPCM – Turns/cm.

Figure 13. (a) Effect of fibre diameter on vertical wicking behaviour of yarn (theoretical). (b) Effect of fibre diameter on vertical wicking behaviour of yarn.
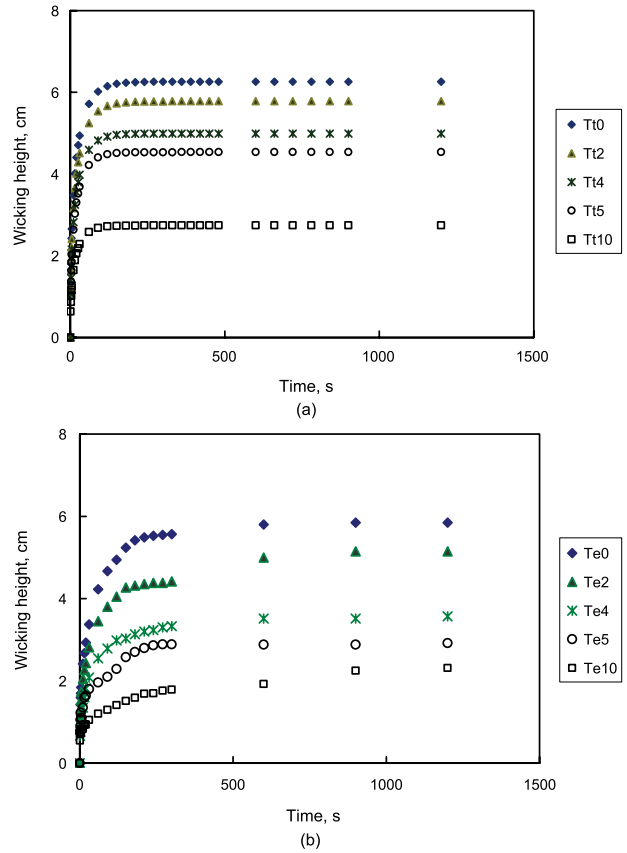

Figure 14. (a) Effect of yarn twist on vertical wicking behaviour of coarse denier circular multi-filament polyester yarn – theoretical. (b) Effect of yarn twist on vertical wicking behaviour of coarse denier circular multifilament polyester yarn – experimental. Tt1 – theoretical (with twist 1 turns/cm) and Tt10 – theoretical (with twist 10 turns/cm). Te1 – experimental (with twist 1 turns/cm) and Te10 – experimental (with twist 10 turns/cm).

change in wicking height with time was much higher than in case of yarn with coarse denier fibre.

Effect of yarn twist

The wicking behaviour of circular normal denier and microdenier filament yarn with increase in twist has been plotted in Figures 14 and 15(b). From the theoretical model it has been observed that with the increase in yarn twist (Figures 14(a) and 15(a)) both in case of normal denier and microdenier multifilament yarn, the equilibrium wicking height and the rate of wicking reduce. Same trend has been observed from the experimental results as well (Figures 14(b) and 15(b)). Symbol Tt_0, Tt_1, Tt_2, Tt_3, Tt_4, Tt_5 and Tt_{10} represent for theoretical wicking value for yarn with twist/cm 0, 1, 2, 3, 4, 5 and 10, respectively; similarly Te_0, Te_1, Te_2, Te_3, Te_4, Te_5 and Te_{10} represent for experimental wicking value for yarn with twist/cm 0, 1, 2, 3, 4, 5 and 10, respectively. In Figure 14(b) for circular normal denier multifilament yarn, the wicking curves have been given for twist 0, 2, 4, 5, 10 turns/cm. In Figure 15(b) wicking curves for

microdenier multifilament yarn for twist 0, 1, 2, 5 and 10 turns/cm have been plotted.

In the same way Te_0, Te_1, Te_2, Te_3, Te_4, Te_5 and Te_{10} represent for experimental wicking value for yarn with twist/cm 0, 1, 2, 3, 4, 5 and 10, respectively. Figure 16(a) and (b) presents a comparison of maximum wicking height calculated from the theoretical model and obtained from the experimental results with the increase in twist/cm (TPCM) of the yarn for circular normal denier (1) and microdenier (2) multifilament polyester yarn.

Effect of fibre profile

Figure 17(a) and (b) presents the effect of fibre shape factor on vertical wicking behaviour of yarn. The values obtained from the theoretical model (Figure 17(a)) as well as from the experimental data (Figure 17(b)) show that yarn with trilobal cross-sectional
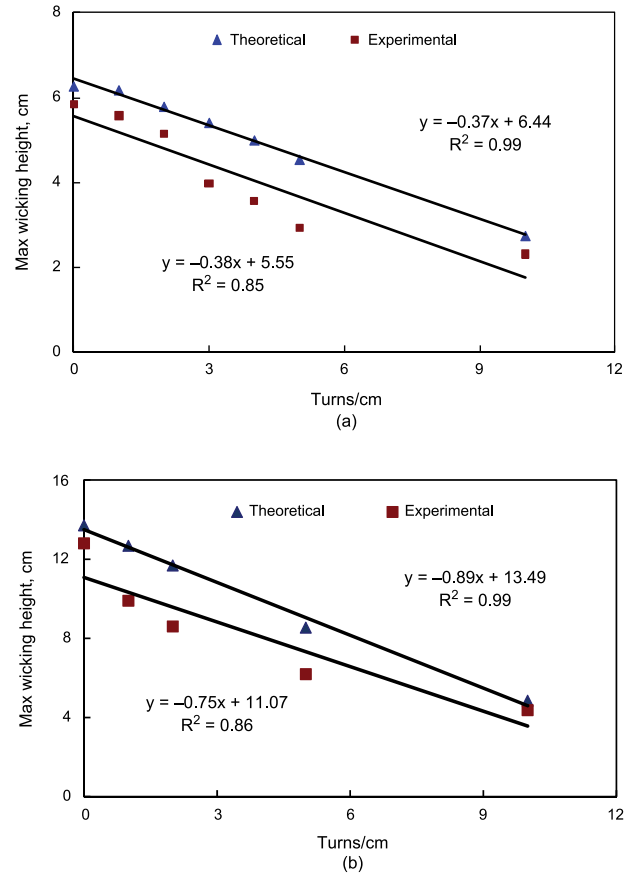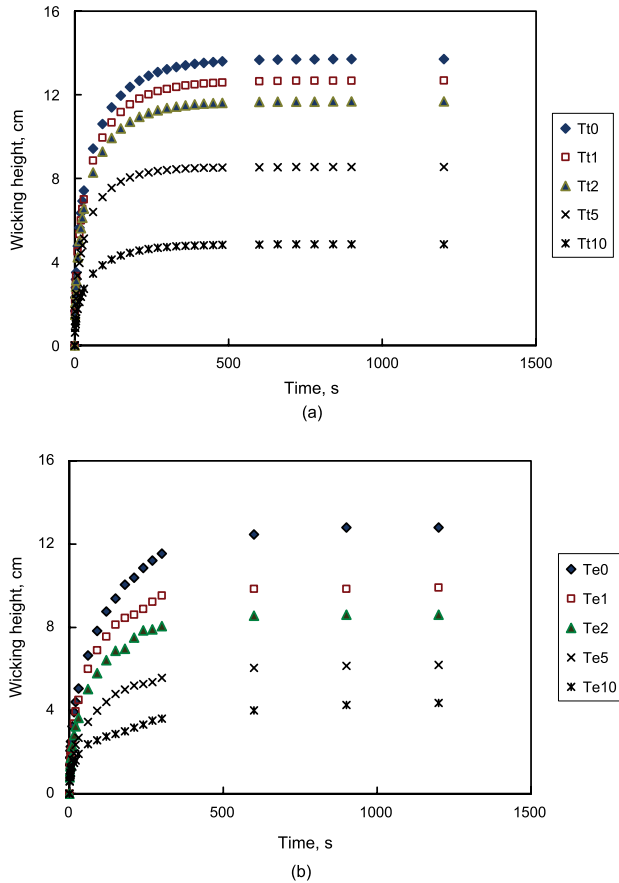
Figure 15. (a) Effect of yarn twist on vertical wicking behaviour of microdenier denier multifilament polyester yarn – theoretical. (b) Effect of yarn twist on vertical wicking behaviour of microdenier denier multifilament polyester yarn – experimental. Tt1 – theoretical (with twist 1 turns/cm) and Tt10 – theoretical (with twist 10 turns/cm). Te1 – experimental (with twist 1 turns/cm) and Te10 – experimental (with twist 10 turns/cm).

Figure 16. (a) Turns/cm vs. maximum wicking height – circular normal denier multifilament yarn. (b) Turns/cm vs. maximum wicking height – microdenier multifilament yarn.

filament offers highest wicking, followed by triangular and circular cross-sectional filaments. Figure 18 presents a comparison of maximum wicking height calculated from the theoretical model and obtained from the experimental results for different shape factor. In both the cases, theoretical and experimental, the equilibrium height follows a linear relation with fibre shape factor.

The results show that the value of wicking height has come always higher from the theoretical results than that have obtained from the experimental data. This may be attributed to the deviation of packing of the fibres from the idealised packing considered in the model. Also, during the experimental study no preventive method has been adopted to avoid the liquid evaporation during wicking, which may have resulted lower equilibrium wicking height than the actual.

Conclusions

- Vertical wicking through yarn structure has been investigated using a model based on macroscopic force balance method. The model can predict the vertical wicking behaviour with reasonable accuracy.
- The model takes care of several parameters like fibre denier, yarn denier, fibre cross-sectional shape and number of fibres in the yarn and yarn twist.
- From the theoretical model, it is predicted that yarn having same linear density but made of more number of fibres (i.e. with smaller denier fibres) will provide higher wicking. The same trend has been observed from the experimental results.
- The model also predicts that with the increase in twist in yarn, its wickability reduces and with the increase in fibre shape factor, the wickability of yarn increases. The experimental verification of the model shows similar trend.
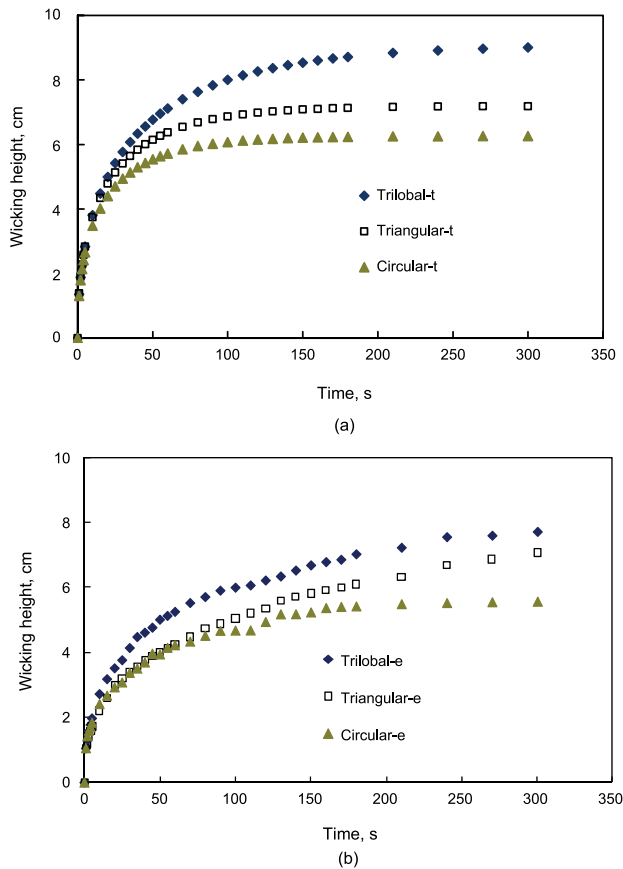
Figure 17. (a) Effect of fibre shape factor on vertical wicking behaviour of yarn – theoretical. (b) Effect of fibre shape factor on vertical wicking behaviour of yarn – experimental. t, theoretical; e, experimental.
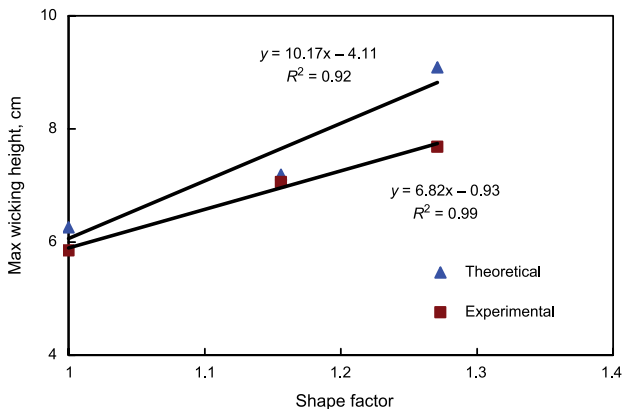

Figure 18. Fibre shape factor vs. maximum wicking height.

- The model does not take care of yarn hairiness, capillary channel discontinuity and liquid absorption phenomenon.

References

Chatterjee, P.K. (1985). *Absorbency.* Amsterdam: Elsevier.

Clark, D.B., & Miller, B. (1978). Liquid transport through fabrics: Wetting and steady-state flow. Part II: Fabric wetting. *Textile Research Journal, 48*(5), 256–260.

Hagen, G. (1839). The flow of water in narrow cylindrical tubes. *Annual Review of Physical Chemistry, 46*, 423–442.

Hearle, J.W.S., Grosberg, P., & Baker, S. (1969). *Structural mechanics of fibres, yarns and fabrics.* New York: Wiley Interscience.

Kamath, Y.K., Hornby, S.B., Weigman, H.D., & Wilde, M.F. (1994). Wicking of spin finishes and related liquids into continuous filament yarns. *Textile Research Journal, 64*(1), 33–40.

Kissa, E. (1996). Wetting and wicking. *Textile Research Journal, 66*(10), 660–668.

Lekner, J. (2007). Viscous flow through pipes of various cross-sections. *European Journal of Physics, 28*, 521–527.

Liu, T., Choi, K., & Li, Y. (2008). Wicking in twisted yarns. *Journal of Colloid and Interface Science, 318*, 134–139.

Lukas, R. (1918). Ueber das Zeitgesetz des kapillaren Aufstiegs von Flussigkeiten. *Kolloidn Zhurnal, 23*, 15–22.

Mao, N., & Russell, S.J. (2000). Directional permeability in homogeneous nonwoven structures. Part I: The relationship between directional permeability and fibre orientation. *Journal of the Textile Institute, 91*(1), 235–258.

Millionshchikov, M.D. (1970). Turbulent flow in pipes of noncircular cross section. *Atomnaya Energiya, 29*(1), 16–18.

Minor, F.M., & Schwartz, A.M. (1960). Pathways of capillary migration of liquids in textile assemblies. *American Dyestuff Reporter, 49*, 37–42.

Neckar, B., & Ibrahim, S. (2003). *Structural theory of fibrous assemblies and yarns.* Liberec: Technical University of Liberec.

Nyoni, A.B., & Brook, D. (2006). Wicking mechanisms in yarns – the key to fabric wicking performance. *Journal of Textile Institute, 97*(2), 119–128.

Palmer, W.B. (1953). The advance of a liquid front along a glass yarn. *Journal of the Textile Institute, 44*, 391–400.

Perwuelz, A., Casetta, M., & Caze, C. (2001). Liquid organisation during capillary rise in yarns: Influence of yarn torsion. *Polymer Testing, 20*, 553–561.

Perwuelz, A., Mondon, P., & Caze, C. (2000). Experimental study of capillary flow in yarn. *Textile of Research Journal, 70*(4), 333–339.

Washburn, E.W. (1921). The dynamics of capillary flow. *Physical Review, 17*, 273.

Wiener, J., & Dejlová, P. (2003). Wicking and wetting in textiles. *Autex Research Journal, 3*(2), 64–71.